

SS-Net: 3D Spatial-Spectral Network for Cerebrovascular Segmentation in TOF-MRA

Chaozhi Yang¹ , Yachuan Li¹, Yun Bai¹, Qian Xiao¹, Zongmin Li^{1()}, Hongyi Li² , and Hua Li³ 

¹ College of Computer Science and Technology, China University of Petroleum (EastChina), Qingdao 266580, China

lizongmin@upc.edu.cn

² Beijing Hospital, Institute of Geriatric Medicine, Chinese Academy of Medical Science, Beijing 100730, China

³ Key Laboratory of Intelligent Information Processing, Institute of Computing Technology, Chinese Academy of Sciences, Beijing 100190, China

Abstract. The extraction of cerebrovascular structure plays a pivotal role in the diagnosis and analysis of various cerebrovascular diseases. However, cerebrovascular segmentation from time-of-flight magnetic resonance angiography (TOF-MRA) volumes remains a challenging task due to the complex topology, slender contour, and noisy background. This paper proposes a 3D SS-Net that combines the spatial and spectral domain features to accurately segment the cerebral vasculature. The SS-Net is based on an end-to-end autoencoder architecture, which incorporates both spatial and a spectral encoders. The spectral encoder branch applies 3D fast Fourier convolution (FFC) to extract global features and frequency domain features in the shallow layers of the network. Furthermore, we introduce cerebrovascular edge supervised information, which enables the network to model the high-frequency variations and distribution patterns of cerebrovascular edges more effectively. Experimental results show that the SS-Net delivers outstanding performance, achieving the DSC of 71.14% on a publicly available dataset and outperforming other 3D deep-learning-based approaches.
Code: github.com/y8421036/SS-Net

Keywords: Cerebrovascular segmentation · Fast Fourier Convolution · 3D U-Net · Edge supervision · TOF-MRA

1 Introduction

Cerebrovascular diseases, such as intracranial aneurysms, arteriovenous malformations, and stenoses, are a significant threat to human health for high incidence, mortality, and disability rates[8]. Time-of-flight magnetic resonance angiography is a non-invasive imaging technique routinely used for evaluating vascular abnormalities without administering contrast. The accurate extraction of the vascular system allows clinicians to support early diagnosis, optimal treatment, and

neurosurgery planning. However, automatic cerebrovascular segmentation from TOF-MRA is challenging due to anatomical variations, sophisticated geometry and shape, and data sparseness (artifacts, noises, low signal-to-noise ratio).

In the last two decades, there have been many model-driven vessel segmentation methods proposed, including active contours[19], tractography[2], shape model[10,24], Hessian matrix filtering[7], and symmetry filtering[23]. These algorithms need detailed design and rely on complicated manual parameter adjustments.

With the rapid development of deep learning technology, data-driven segmentation methods achieve better performance. Phellan et al.[13] utilized the 2D convolutional neural network (CNN) to segment the cerebral vessel slices. Sanches et al.[14] proposed the Uception segmentation model that combines inception [17] and 3D U-Net [5]. Wang et al.[18] constructed a joint convolutional embedding space where computed joint cerebrovascular probabilities. Mou et al.[12] presented a generic and unified CNN for segmentating curvilinear structures, including 2D and 3D vasculatures. Chen et al.[3] proposed a GAN-based method that maps the TOF-MRA images to cerebral vessels. However, the above methods neglect to prioritize the extraction of cerebrovascular edges that are essential for vessel connectivity. Although several studies[21,1] focus on edge information, they leave out practical features in the spectral domain, which existing spatial neural networks may not extract.

The high-frequency variations of cerebrovascular edges in TOF-MRA images make edge features suitable to be extracted in the spectral domain. In this paper, we combine the spatial and spectral features to segment the brain vessels. First, we design a spectral encoder as another branch of 3D U-Net to extract frequency domain features and process global information. Cerebrovascular edge labels are then introduced as additional supervision, allowing the SS-Net to focus more on edge features in both the spatial and spectral domains. The contributions of this paper are summarized as follows:

1. To our knowledge, SS-Net is the first 3D cerebrovascular segmentation network combining spatial and spectral domain features.
2. We introduce edge supervision to improve the spectral encoder's ability to learn the cerebrovascular edges' frequency domain features.
3. Experimental results on a public dataset demonstrate that the SS-Net outperforms other deep learning methods quantitatively and qualitatively.

2 Method

2.1 The Overall Framework of SS-Net

The proposed SS-Net consists of several components: a spatial encoder, a spectral encoder, a spatial decoder, skip connections, and double-task head. The core unit of the proposed spectral encoder is the Fast Fourier Convolution[4,16,6], which learns cerebrovascular features from the frequency domain and processes global

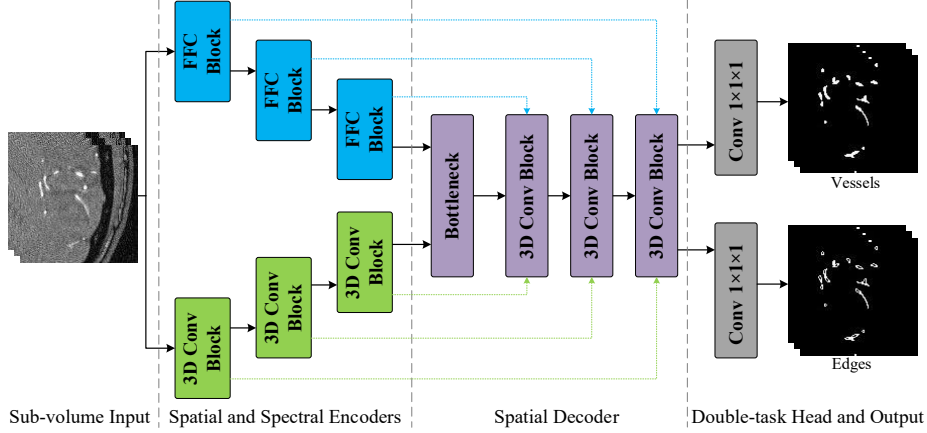


Fig. 1. Overview of the proposed SS-Net.

features that the spatial convolution may miss. The overall framework of SS-Net is shown in Fig. 1).

3D Spatial Encoder. Our spatial encoder contains the same skip connections as 3D U-Net’s encoder to complement the details lost by downsampling. The number of downsampling operations and 3D convolution blocks is both 3. A $3 \times 3 \times 3$ convolutional kernel, a 3D Batch Normalization (BN), and an activation function (ReLU) are sequentially combined to form a 3D convolution block in our spatial encoder. The downsampling operation adopts a 3D Max Pooling (MP), and the kernel size of the MP is 2. The input of the first 3D convolution block is a cropped sub-volume from the original image, and the output is fed to the next block.

3D Spectral Encoder. Similar to the spatial encoder, the spectral encoder has skip connections, downsampling, and sub-volume input. Three FFC blocks process the input to obtain the output. Each FFC block contains regular convolutions for processing local information and the spectral transform for processing global information. The core of the spectral transform is the Fast Fourier Transform (FFT) and the inverse Fast Fourier Transform (IFFT). The FFT converts image features into frequency domain features. The IFFT does the opposite. Updating a single value affects all the original data globally in the frequency domain transformed by FFT. Therefore, this gives the FFC-generated features image-wide receptive fields even in the shallow layers of the network.

3D Spatial Decoder. The spatial decoder contains a bottleneck layer and three 3D convolution blocks. The bottleneck layer concatenates the output features of the two encoders and learns the semantic features using a $3 \times 3 \times 3$ convolutional kernel. The new features are upsampled and passed to a 3D convolutional block similar to the spatial encoder. Each 3D convolutional block fuses features from previous decoder blocks with features from skip connections to learn higher-level features. In order to restore the feature map to the size of

the sub-volume input, the spatial decoder employs three upsampling operations based on transpose convolution.

Double-task Head. The output of the decoder is processed by the double-task head to obtain a vessel segmentation map and an edge segmentation map, respectively. Both task heads have the same architectural design, consisting of a $1 \times 1 \times 1$ convolution kernel and an activation function (sigmoid).

2.2 3D Spectral Encoder Components

3D FFC Block. As shown in Fig. 2(a), the FFC Block divides the input equally into two parts by the number of channels and feeds to two inter-connected paths. In the first FFC block, since the input is a sub-volume of the original image, the number of channels of the global path is set to 0. The local path conducts ordinary convolution, and the global path uses the spectral transform to operate in the spectral domain. Since each path captures complementary information with a different receptive field, the two paths exchange information through multi-scale fusion. Then the features are fed into a 3D BN, a ReLU, and a 3D MP. Finally, the features of the two paths are concatenated at the channel level and used as the output of the FFC Block.

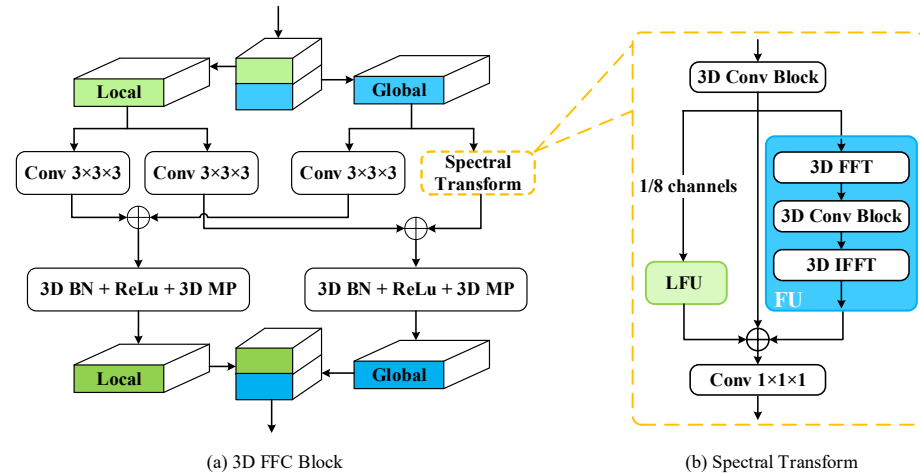


Fig. 2. The design of fast Fourier convolution.

Spectral Transform. Spectral transform extracts frequency domain features and allows the network to account for the global context starting from the shallow layer. In Fig. 2(b), after the input features are applied to a 3D convolutional block with a kernel size of 1, the new features are passed to three paths: i) Fourier Unit (FU), ii) residual connection, and iii) Local Fourier Unit (LFU). Note that the LFU path requires only one-eighth of the channels. The outputs of the three paths are fused and fed to a $1 \times 1 \times 1$ convolution kernel.

FU and LFU. The FU first utilizes FFT to convert spatial features into real and imaginary parts. These two parts are stacked and fed to a 3D convolutional block with a kernel size of 1. The generated features are split into two parts as real and imaginary. They are then converted back to image features by IFFT. The FFT can be applied only to real-valued signals, and the IFFT ensures that the output is real valued. To capture semi-local information, we devise LFU, whose pipeline is shown in Fig. 3. The key difference between LFU and FU is a split-concatenate-repeat step, which halves three spatial dimensions of input feature maps and processes eight small feature maps. Standard FU is then applied to stacked feature maps. The generated features are shifted and repeated to restore to the initial resolution.

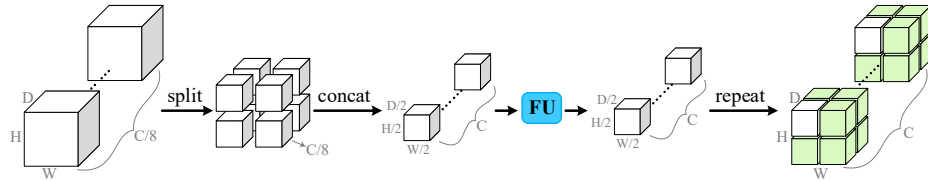


Fig. 3. Illustration of the computational pipeline of local Fourier unit.

2.3 Loss function

Three different loss functions train the vessel and edge segmentation tasks. For the cerebrovascular segmentation task, the loss function $L_{cere} = L_{BCE} + \lambda_1 L_{dice}$ is defined as the combination of the Binary Cross-Entropy (BCE) loss and the dice coefficient loss:

$$L_{dice} = 1 - \frac{2 \sum_{j=1}^N p_j g_j + \epsilon}{\sum_{j=1}^N p_j + \sum_{j=1}^N g_j + \epsilon} \quad (1)$$

$$L_{BCE} = -\frac{1}{N} \sum_{j=1}^N g_j \log(p_j) + (1 - g_j) \log(1 - p_j) \quad (2)$$

where p_j and g_j indicate the predicted probability and ground truth of the j -th voxel within an input volume patch. N is the number of voxels. The parameter ϵ (set as 1) is the Laplace smoothing factor that guarantees numerical stability. The λ_1 is the weight balance parameter between L_{dice} and L_{BCE} , which is empirically set as 1.

For the edge segmentation task, due to the problem of severe class imbalance, the well-known focal loss is used, defined as follows:

$$L_{edge} = L_{focal} = \frac{1}{N} \sum_{j=1}^N -\alpha(1 - p_j)^\gamma \log(p_j) \quad (3)$$

where α and γ are adjustable factors and are set to 0.25 and 2, respectively. Therefore, the proposed SS-Net can be jointly optimized by minimizing the joint loss $L = L_{cere} + \lambda_2 L_{edge}$ in an end-to-end manner. The hyper-parameter λ_2 controls the influence of the edge part and is empirically set to 0.5.

3 Experimental Results

3.1 Datasets and Pre-processing

We conduct our experiments on the MIDAS¹ dataset. The MIDAS contains 42 TOF-MRA volumes of different subjects, acquired by a Siemens Allegra head-only 3T MR system. The intra-cranial vessel annotations are obtained via the TubeTK toolkit. The voxel spacing for the MRA images is $0.5 \times 0.5 \times 0.8 \text{ mm}^3$ with a volume size of $448 \times 448 \times 128$ voxel.

We apply the BET[9] of the MR-based skull-stripping algorithm to extract the pure brain region from each volumetric data. To reduce the difference of intensity distribution among volumes, each TOF-MRA volume is normalized by min-max scaling. A 6-neighborhood filter generates the one-voxel-thick cerebrovascular edge labels given the ground-truth volume G of the input TOF-MRA volume I . The $N(i)$ denotes the 6-neighbor voxels of i . We define the set of voxels E on the cerebrovascular edge as:

$$E_i = \{i \mid g_i = 1, \exists x \in N(i), g_x = 0\} \quad (4)$$

3.2 Implementation Details

In this work, we randomly extract training sub-volumes with a specified size of $96 \times 96 \times 96$ for each case. The sliding window strategy of no overlapping is employed during testing. It is worth noting that we combine the predicted values of all sub-volumes for evaluation. The MIDAS dataset's random training/validation/testing case split is 36/2/4.

The proposed network adopts the Adam optimizer with an initial learning rate of 0.0005 with 0.5 as the learning decay factor. The network is implemented on PyTorch with an NVIDIA GeForce GTX TITAN X GPU (12G RAM). Following previous work[20], we adopted the poly learning rate method with a power of 0.9.

We compare with other deep learning segmentation models, including Uception[15], RE-Net[22] and CS²-Net[12] for 3D cerebrovascular segmentation, and two state-of-the-art 3D FCNs for medical volume segmentation, such as 3D UNet[5] and V-Net[11].

For evaluating the segmentation performance of our network, some well-known metrics were introduced: Dice Similarity Coefficient (DSC), Sensitivity (SE), Specificity (SP), Precision (PR), and Accuracy (ACC). Since the above metrics are insensitive to the foreground edge, the 95th Hausdorff Distance

¹ <https://public.kitware.com/Wiki/TubeTK/Data>

(HD95) and the Average Hausdorff Distance (AHD) were adopted better to evaluate the segmentation results of the cerebral vasculature. The HD95 is the 95 percentile of the Hausdorff distance (HD). These metrics are defined as follows:

$$\left\{ \begin{array}{l} DSC = \frac{2TP}{TP+2TP+FN} \\ SE = \frac{TP}{TP+FN} \\ SP = \frac{TN}{FP+TN} \\ PR = \frac{TP}{TP+FP} \\ ACC = \frac{TP+TN}{TP+TN+FP+FN} \\ HD = \max \left\{ \max_{p \in P} \min_{g \in G} \|p - g\|, \max_{g \in G} \min_{p \in P} \|g - p\| \right\} \\ AHD = \frac{1}{2} \left\{ \frac{1}{\#P} \sum_{p \in P} \min_{g \in G} \|p - g\| + \frac{1}{\#G} \sum_{g \in G} \min_{p \in P} \|g - p\| \right\} \end{array} \right. \quad (5)$$

in which TP, FP, FN, and TN are true positive, false positive, false negative, and true negative in the confusion matrix. The P and G denote the voxel sets of prediction and ground truth, respectively. The $\#$ represents the number of voxels in a set. The symbol of $\|\cdot\|$ is taken as the Euclidean distance between two voxels.

3.3 Ablation Study

The main contribution of our network is to design the 3D spectral encoder and introduce the edge auxiliary task for improving cerebrovascular segmentation accuracy. To verify the efficacy of these modules, we conduct ablation experiments on the MIDAS dataset. Note that the baseline is 3D U-Net. In addition, we compare the performance of triple downsampling and quadruple downsampling based on SS-Net.

The results of the ablation experiment are summarized in Table 1. Introducing any of the two modules achieves better performance than the baseline. In terms of the DSC indicator, adding the 3D spectral decoder alone improved the score by 5.28%, and introducing the edge task alone improved it by 3.64%. The SS-Net achieves the highest scores in most metrics by incorporating both modules. Specifically, SS-Net improved by 6.04% and 1.91mm in DSC and $HD95$, respectively, compared with the baseline network. We believe that the edge segmentation assistance task helps to enhance the vessel edge features and reduce the effect of background noise. Moreover, based on our proposed framework, better results are obtained using three times downsampling.

3.4 Quantitative and Qualitative Analysis

To qualitatively compare the segmentation results of the proposed method with other deep learning vessel segmentation methods, Fig. 4 shows the segmentation examples of 3D views on the test set. The 3D U-Net has poor segmentation performance. The V-Net generates more false negative errors. The amount of detached false positive errors produced by SS-Net is apparently less than that of other compared methods. The SS-Net performs well in segmenting multi-size

Table 1. Effect of modular ablation experiments on segmentation index of the cerebral vasculature. Bold denotes the best results.

Methods	SE(%) \uparrow	SP(%) \uparrow	DSC(%) \uparrow	HD95(mm) \downarrow	AHD(mm) \downarrow
Baseline	65.97 \pm 3.96	99.83 \pm 0.02	65.10 \pm 3.31	10.26 \pm 2.37	1.2560 \pm 0.25
Baseline + Spectral Encoder	66.61 \pm 2.54	99.90 \pm 0.02	70.38 \pm 2.91	9.32 \pm 2.48	1.0601 \pm 0.18
Baseline + Edge Task	66.37 \pm 2.59	99.84 \pm 0.03	68.74 \pm 2.71	10.39 \pm 2.01	1.2045 \pm 0.28
SS-Net with 4 downsampling	64.23 \pm 2.38	99.90 \pm 0.02	68.32 \pm 2.81	10.57 \pm 2.04	1.1243 \pm 0.17
SS-Net	67.92\pm2.66	99.91\pm0.01	71.14\pm2.76	8.35\pm2.18	1.0416\pm0.23

vessel branches and maintaining the continuity of the vessels. Overall, SS-Net yields more complete segmentation of the whole cerebrovascular structure. We believe that better performance comes from the contribution of vessel edges and global features.

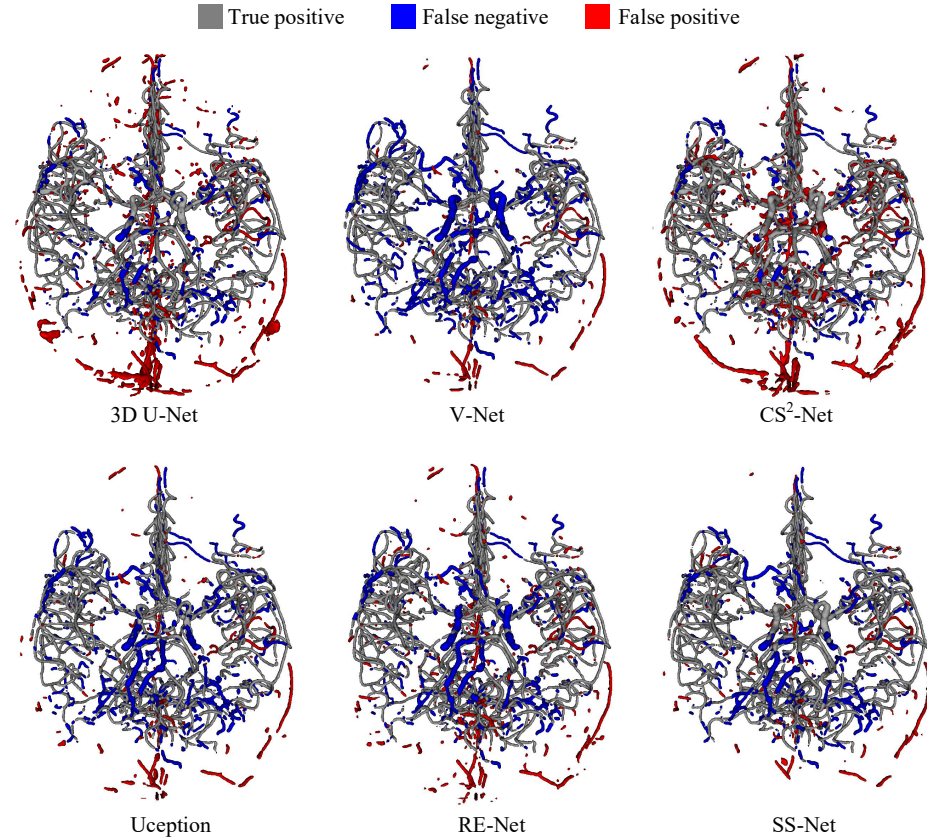


Fig. 4. Visual comparison of cerebrovascular segmentation results produced by the SS-Net and other deep-learning methods from a 3D view.

The evaluation scores in Table 2 reinforce the above findings. In terms of DSC metrics, SS-Net is 6.04%, 9.11%, 5.7%, 8.36%, and 4.37% higher than 3D U-Net, V-Net, CS²Net, Uception, and RE-Net, respectively. It can be seen that the proposed SS-Net outperformed the other methods and achieved the highest scores in all metrics. Overall, the proposed SS-Net excels in cerebral vascular segmentation from 3D TOF-MRA volumes.

Table 2. Segmentation results obtained by different methods.

Metrics	3D U-Net[5]	V-Net[11]	CS ² -Net[12]	Uception[14]	RE-Net[22]	SS-Net
SE(%)↑	65.97±3.96	60.35±3.33	66.17±1.80	56.39±4.64	64.51±4.40	67.92±2.66
SP(%)↑	99.83±0.02	99.90±0.01	99.79±0.02	99.89±0.02	99.89±0.01	99.91±0.01
PR(%)↑	67.36±3.09	69.32±3.06	57.60±4.57	70.82±3.23	67.77±4.04	74.70±3.15
ACC(%)↑	99.75±0.02	99.73±0.03	99.70±0.02	99.75±0.01	99.75±0.02	99.79±0.03
DSC(%)↑	65.10±3.31	62.03±2.70	65.44±3.25	62.78±2.22	66.77±3.13	71.14±2.76
HD95(mm)↓	10.26±2.37	9.53±0.14	10.46±1.76	10.00±0.79	9.50±0.88	8.35±2.18
AHD(mm)↓	1.2560±0.25	1.2526±0.17	1.3358±0.28	1.1990±0.16	1.0676±0.12	1.0416±0.23

4 Conclusion

In this work, we have proposed a 3D convolution network, SS-Net, to segment cerebrovascular structure from TOF-MRA volumes. Our FFC-based spectral encoder obtains global information more quickly and efficiently than an encoder containing ordinary convolution. In addition, by introducing cerebral vascular edge supervision, the spectral encoder can model the distribution of cerebrovascular edge, improving vascular connectivity. Our SS-Net combines image and frequency domain features to extract more accurate cerebrovascular structure. Experimental results based on publicly available datasets show that the proposed method significantly improves the accuracy of cerebrovascular segmentation.

Acknowledgements This work is partly supported by National Key R&D Program of China (Grant no. 2019YFF0301800), National Natural Science Foundation of China (Grant no. 61379106, 61806199), the General Research Projects of Beijing Educations Committee in China (Grant no. KM201910005013), the Shandong Provincial Natural Science Foundation (Grant nos.ZR2015FM011).

References

1. Banerjee, S., Toumpanakis, D., Dhara, A.K., Wikström, J., Strand, R.: Topology-aware learning for volumetric cerebrovascular segmentation. In: 2022 IEEE 19th International Symposium on Biomedical Imaging. pp. 1–4 (2022). <https://doi.org/10.1109/ISBI52829.2022.9761429>

2. Cetin, S., Demir, A., Yezzi, A., Degertekin, M., Unal, G.: Vessel tractography using an intensity based tensor model with branch detection. *IEEE Transactions on Medical Imaging* **32**(2), 348–363 (2013). <https://doi.org/10.1109/TMI.2012.2227118>
3. Chen, Z., Xie, L., Chen, Y., Zeng, Q., ZhuGe, Q., Shen, J., Wen, C., Feng, Y.: Generative adversarial network based cerebrovascular segmentation for time-of-flight magnetic resonance angiography image. *Neurocomputing* **488**, 657–668 (2022)
4. Chi, L., Jiang, B., Mu, Y.: Fast fourier convolution. In: Larochelle, H., Ranzato, M., Hadsell, R., Balcan, M., Lin, H. (eds.) *Advances in Neural Information Processing Systems*. vol. 33, pp. 4479–4488. Curran Associates, Inc. (2020)
5. Çiçek, Ö., Abdulkadir, A., Lienkamp, S.S., Brox, T., Ronneberger, O.: 3d u-net: learning dense volumetric segmentation from sparse annotation. In: *International conference on medical image computing and computer-assisted intervention*. pp. 424–432. Springer (2016)
6. Farshad, A., Yeganeh, Y., Gehlbach, P., Navab, N.: Y-net: A spatirospectral dual-encoder network for medical image segmentation. In: *Medical Image Computing and Computer Assisted Intervention–MICCAI 2022: 25th International Conference, Singapore, September 18–22, 2022, Proceedings, Part II*. pp. 582–592. Springer (2022)
7. Frangi, A.F., Niessen, W.J., Vincken, K.L., Viergever, M.A.: Multiscale vessel enhancement filtering. In: *International Conference on Medical Image Computing and Computer-Assisted Intervention* (1998)
8. Han, H., Zhang, R., Liu, G., Qiao, H., Chen, Z., Liu, Y., Chen, X., Li, D., Wang, Y., Zhao, X.: Reduction of cerebral blood flow in community-based adults with sub-clinical cerebrovascular atherosclerosis: A 3.0t magnetic resonance imaging study. *NeuroImage* **188**, 302–308 (2019). <https://doi.org/https://doi.org/10.1016/j.neuroimage.2018.12.021>
9. Jenkinson, M., Pechaud, M., Smith, S., et al.: Bet2: Mr-based estimation of brain, skull and scalp surfaces. In: *Eleventh Annual Meeting of the Organization for Human Brain Mapping*. vol. 17, p. 167. Toronto. (2005)
10. Liao, W., Rohr, K., Wörz, S.: Globally optimal curvature-regularized fast marching for vessel segmentation. In: Mori, K., Sakuma, I., Sato, Y., Barillot, C., Navab, N. (eds.) *Medical Image Computing and Computer-Assisted Intervention – MICCAI 2013*. pp. 550–557. Springer Berlin Heidelberg, Berlin, Heidelberg (2013)
11. Milletari, F., Navab, N., Ahmadi, S.A.: V-net: Fully convolutional neural networks for volumetric medical image segmentation. In: *2016 fourth international conference on 3D vision*. pp. 565–571. IEEE (2016)
12. Mou, L., Zhao, Y., Fu, H., Liu, Y., Cheng, J., Zheng, Y., Su, P., Yang, J., Chen, L., Frangi, A.F., et al.: Cs2-net: Deep learning segmentation of curvilinear structures in medical imaging. *Medical Image Analysis* **67**, 101874 (2021)
13. Phellan, R., Peixinho, A., Falcão, A., Forkert, N.D.: Vascular segmentation in tof mra images of the brain using a deep convolutional neural network. In: *MICCAI workshops on Large-Scale Annotation of Biomedical data and Expert Label Synthesis and Computing and Visualization for Intravascular Imaging and Computer Assisted Stenting*, pp. 39–46. Springer (2017)
14. Sanches, P., Meyer, C., Vigon, V., Naegel, B.: Cerebrovascular network segmentation of mra images with deep learning. In: *2019 IEEE 16th International Symposium on Biomedical Imaging*. pp. 768–771. IEEE (2019)
15. Sanches, P., Meyer, C., Vigon, V., Naegel, B.: Cerebrovascular network segmentation of mra images with deep learning. In: *2019 IEEE 16th International Symposium on Biomedical Imaging*. pp. 768–771. IEEE (2019)

16. Suvorov, R., Logacheva, E., Mashikhin, A., Remizova, A., Ashukha, A., Silvestrov, A., Kong, N., Goka, H., Park, K., Lempitsky, V.: Resolution-robust large mask inpainting with fourier convolutions. In: 2022 IEEE/CVF Winter Conference on Applications of Computer Vision. pp. 3172–3182 (2022). <https://doi.org/10.1109/WACV51458.2022.00323>
17. Szegedy, C., Ioffe, S., Vanhoucke, V., Alemi, A.A.: Inception-v4, inception-resnet and the impact of residual connections on learning. In: Thirty-first AAAI conference on artificial intelligence (2017)
18. Wang, Y., Yan, G., Zhu, H., Buch, S., Wang, Y., Haacke, E.M., Hua, J., Zhong, Z.: Jointvesselnet: Joint volume-projection convolutional embedding networks for 3d cerebrovascular segmentation. In: International Conference on Medical Image Computing and Computer-Assisted Intervention. pp. 106–116. Springer (2020)
19. Yang, X., Cheng, K.T., Chien, A.: Geodesic active contours with adaptive configuration for cerebral vessel and aneurysm segmentation. In: 2014 22nd International Conference on Pattern Recognition. pp. 3209–3214 (2014). <https://doi.org/10.1109/ICPR.2014.553>
20. Zhang, H., Dana, K., Shi, J., Zhang, Z., Wang, X., Tyagi, A., Agrawal, A.: Context encoding for semantic segmentation. In: Proceedings of the IEEE conference on Computer Vision and Pattern Recognition. pp. 7151–7160 (2018)
21. Zhang, H., Xia, L., Song, R., Yang, J., Hao, H., Liu, J., Zhao, Y.: Cerebrovascular segmentation in mra via reverse edge attention network. In: International Conference on Medical Image Computing and Computer-Assisted Intervention. pp. 66–75. Springer (2020)
22. Zhang, H., Xia, L., Song, R., Yang, J., Hao, H., Liu, J., Zhao, Y.: Cerebrovascular segmentation in mra via reverse edge attention network. In: International Conference on Medical Image Computing and Computer-Assisted Intervention. pp. 66–75. Springer (2020)
23. Zhao, Y., Zheng, Y., Liu, Y., Zhao, Y., Luo, L., Yang, S., Na, T., Wang, Y., Liu, J.: Automatic 2-d/3-d vessel enhancement in multiple modality images using a weighted symmetry filter. *IEEE Transactions on Medical Imaging* **37**(2), 438–450 (2018). <https://doi.org/10.1109/TMI.2017.2756073>
24. Zhou, S., Li, N., Zhang, B., Wang, C., Wu, Z., Yang, J., Chien, A.: Statistical intensity- and shape-modeling to automate cerebrovascular segmentation from tof-mra data. In: Medical Image Computing and Computer Assisted Intervention – MICCAI 2019: 22nd International Conference. p. 164–172. Springer-Verlag, Berlin, Heidelberg (2019). https://doi.org/10.1007/978-3-030-32245-8_19